Discrimination of crop types with TerraSAR-X-derived information

Rei Sonobe[a*], Hiroshi Tani[b], Xiufeng Wang[b], Nobuyuki Kobayashi[c] and Hideki Shimamura[d]

[a] JSPS Research Fellow / Graduate School of Agriculture. Hokkaido University, Sapporo, Hokkaido 060-8589, Japan

[b] Research Faculty of Agriculture. Hokkaido University, Sapporo, Hokkaido 060-8589, Japan

[c] Smart Link Hokkaido, Iwamizawa, Hokkaido 068-0034, Japan

[d] PASCO Corporation, Meguro-Ku, Tokyo 153-0043, Japan

*Corresponding author: Tel +81-11-706-3695.

E-mail address: reysnb@gmail.com (R. Sonobe).

Abstract

Although classification maps are required for management and for the estimation of agricultural disaster compensation, those techniques have yet to be established. This paper describes the comparison of three different classification algorithms for mapping crops in Hokkaido, Japan, using TerraSAR-X (including TanDEM-X) dual-polarimetric data. In the study area, beans, beets, grasslands, maize, potatoes and winter wheat were cultivated. In this study, classification using TerraSAR-X-derived information was performed. Coherence values, polarimetric parameters and gamma nought values were also obtained and evaluated regarding their usefulness in crop classification. Accurate classification may be possible with currently existing supervised learning models. A comparison between the classification and regression tree (CART), support vector machine (SVM) and random forests (RF) algorithms was performed. Even though J-M distances were lower than 1.0 on all TerraSAR-X acquisition days, good results were achieved (e.g., separability between winter wheat and grass) due to the characteristics of the machine learning algorithm. It was found that SVM performed best, achieving an overall accuracy of 95.0% based on the polarimetric parameters and gamma nought values for HH and VV polarizations. The misclassified fields were less than 100 a in area and 79.5-96.3% were less than 200 a with the exception of grassland. When some feature such as a road or windbreak forest is present in the TerraSAR-X data, the ratio of its extent to that of the field is relatively higher for the smaller fields, which leads to misclassifications.

Keywords: classification, random forest, support vector machine, TerraSAR-X

1. Introduction

Crop type classification maps are useful for estimating the amount and type of crops harvested in a certain area or for determining agricultural disaster compensation. To managers in the agricultural field, the ability to generate crop type classification maps without concurrent training data is useful for reducing labour costs and eliminating the need for the preliminary collection of information. Optical remote sensing is one of the most attractive options for obtaining biomass information, as currently available sensors offer fine spatial and spectral resolutions (Sarker and Nichol 2011). Some optical satellites such as the Landsat have also been used for crop type classification (Hartfield et al. 2013; Mishra and Crews 2014). A significant amount of information about soil and vegetation parameters has also been obtained by microwave remote sensing such as synthetic aperture radar (SAR) systems. The latter technique is seeing increased use in the management of land and water resources for agricultural applications (Fontanelli et al. 2013). This is because unlike passive systems, SAR systems are not subject to atmospheric influences or weather conditions, which makes them suitable for a multi-temporal classification approach (Bargiel and Herrmann 2011). An increasing amount of studies on rice monitoring and mapping is employing SAR data. The results of these studies have generally found that there are high correlations between backscattering coefficients, plant height and age. The backscattering coefficient is a function of the geometric and dielectric properties of the target and the amount of biomass in the cultivated areas, allowing the distinguishing of different types of temporal changes with multi-temporal SAR data. The first large backscatter intensity change occurs as a result of ploughing and seeding. Subsequent smaller changes are mainly due to variations of biomass and plant water content, or to changes in plant structure in the case of X-band SAR data. Harvesting causes large backscatter intensity changes. However, there are times when no backscatter intensity change is detected despite the presence of geometric changes, typically in areas of dense vegetation such as grassland (Macelloni et al., 2001). Coherence with repeat-pass SAR interferometry is useful for determining sensitivity to state changes in fields. Coherence decay due to crop growth has been observed, although smaller changes were connected to variations in soil moisture and vegetation water content. These observations enhance the potential of InSAR coherence in the estimation of crop parameters during the growing season (Blaes and Defourny 2003). When combined with texture parameters, coherence is useful for forest classification (Liesenberg and Gloaguen 2013). Accordingly, coherence clearly has potential in crop type classification, which was evaluated in the present study.

In this study, HH and VV polarization data of the X-band from TerraSAR-X was used. Following the launch of TerraSAR-X on June 15, 2007, X-band SAR data is now widely available. The objective of the TerraSAR-X mission was to develop an operational spaceborne X-band synthetic aperture radar (SAR) system to produce various processed data for commercial and scientific use. TerraSAR-X delivers X-band SAR data of high geometric accuracy at a high spatial resolution of 2.5-6 m in a 30 km swath in Stripmap mode (Ager and Bresnahan 2009). Polarimetric parameters are also available in this dataset.

Classification using polarimetric parameters has been performed in previous studies. Most studies have, however, focused on land use and land cover classification using quad-pol (fully polarimetric) SAR data (Liu et al. 2013; Loosvelt et al. 2012; Uhlmann and Kiranyaz 2014). In this study, crop classifications using the polarimetric parameters obtained from the TerraSAR-X dual-polarimetric data for HH and VV polarization were examined. The main objective was to evaluate the potential of Terra-SAR-X data for crop type classification and crop map generation, without the use of concurrent training data.

2. Data and methods

2.1. Study area and field work

The study area was a farming area in western Tokachi Plain, Hokkaido, Japan (extent: 142°55′12″ to 143°05′51″E, 42°52′48″ to 43°02′42″N). In total, 5089 fields (1023 bean fields, 616 beet fields, 629 grasslands, 592 maize fields, 704 potato fields and 1525 winter wheat fields) were monitored using TerraSAR-X/TanDEM-X. Average field size was 220 a, ranging from 0.01 ha to 18.0 ha. The cultivation calendar for the crops in this study area is shown in Table 1.

All fields were buffered inward by 10 m to account for field shape. The buffers were used to avoid selecting training pixels from the edge of a field, which would create a mixed signal and affect the accuracy assessment. We used a stratified random sampling approach to select approximately 20% of the crop fields for training samples. The number of samples for each crop type was determined based on the percentage of fields in the area. The remaining 80% of fields were used to perform the accuracy assessment. Table 2 represents the numbers of fields of each crop type.

2.2. SAR data

The whole processing workflow is illustrated in Figure 1. We used 16 scenes of TerraSAR-X and TanDEM-X data (Table 3) obtained as Single-look Slant range Complex (SSC) with dual-polarized StripMap mode (HH and VV polarization). The SARs used in this study area are side-looking SARs based on active phased array antenna technology. They are situated in a sun-synchronous dawn-to-dusk orbit with an 11 day cycle, at an altitude of 514 km above the equator (Roth et al. 2004). When calculating coherence, only adjacent pairs were used, as it was found that InSAR quality was low if the time interval between subsequent observations was more than 22 days.

The two polarimetric parameters, average alpha angle and scattering entropy, were obtained using the European Space Agency's (ESA) PolSARpro SAR Data Processing Educational Tool (Pottier et al. 2009). They were orthorectified using the Alaska Satellite Facility's MapReady Remote Sensing Toolkit (Gens and Logan 2003), the 10 m mesh DEM produced by the Geospatial Information Authority of Japan (GSI) and the Earth Gravitational Model 2008 (EGM2008). The

PolSARPro was developed under contract to the ESA in response to recommendations made at the PolInSAR 2003 workshop in Frascati, Italy. The MapReady Remote Sensing Toolkit was developed by the Alaska Satellite Facility and exports data in GeoTIFF format. Its processing flow includes terrain correction of SAR data using a digital elevation model (DEM) to remove the distortions caused by the side-looking geometry, geocoding into a number of pre-defined standard map projections, and exporting in GeoTIFF format (Gens et al. 2013). To compensate for spatial variability and to avoid problems related to uncertainty in georeferencing, average values of SAR data were calculated for the fields and for each observation using field polygons (shape file format) provided by Tokachi Nosai (http://www.tokachi-nosai.or.jp/). These processes were conducted using ERDAS IMAGINE version 14.0 distributed by Intergraph Corporation.

2.3. Classification algorithm and evaluation

Jeffries-Matusita (J-M) distances (Richards, 1999) were calculated to compare statistical separability among crop types. J-M distance measurements take values from 0 to 2.0 and indicate the degree to which the two selected crop types are statistically separated. As a general rule, if the J-M value is greater than 1.9, then separation is good. If the J-M is between 1.7 and 1.9 then separation is fairly good.

In earlier studies, the classification and regression tree (CART) algorithm was used to identify crops such as alfalfa, corn, cotton, grain, melon orchards and sorghum from Landsat Thematic Mapper (TM) image data(Hartfield et al. 2013). This algorithm achieved an overall accuracy of 87–92% using data acquired in 2008. Using training data from one year and applying it to another year for classification purposes resulted in an overall accuracy of 71–83%, although accuracies were consistently greater than 85% for some crops. In addition to CART, two widely used supervised learning models – support vector machine (Bovolo et al. 2010; Foody and Mathur 2004;

Lizarazo 2008; Pal 2008) and random forest (Duro et al. 2012; Gislason et al. 2006; Kavzoglu and Colkesen 2013; Pal 2005; Rodriguez-Galiano et al. 2012) – were used in this study.

The Support Vector Machine algorithm is based on fitting a logistic distribution to the output values of the decision functions of classifiers and using quadratic optimization to obtain class probabilities (Chang et al. 2011). In this study, the Gaussian Radial Basis Function (RBF) kernel was applied. There are two parameters that control the flexibility of the classifier: the regularization parameter C and the kernel bandwidth γ. If the C value is too large, we have a high penalty for no separable points and we may store many support vectors and over fit. If it is too small, we may have under fitting. It controls the trade-off between errors of the SVM on training data and margin maximization ($C = \infty$ leads to hard margin SVM). The γ value defines how far the influence of a single training example reaches, with low values meaning 'far' and high values meaning 'close'. Optimal parameters for flexibility control were determined through a grid search in the bivariate parameter space. The parameter space was discretized along 2^x, where $x = -1$ to 8 for the regularization parameter C and $x = -12$ to 0 for the kernel bandwidth γ. Both parameters were determined using the k-fold cross-validation technique. The grid search was used to minimize the misclassification error rate. K-fold cross-validation was also used to assess classifier performance (Puertas et al. 2013). This technique repeatedly generates training and test data sets from a reference sample with known land cover class membership. It is used for model validation and consists of partitioning the data into k equally-sized subsets (here, $k = 10$). A classifier is trained on all except one of these subsets and then evaluated on the excluded subset. Accuracy measures are averaged over all test datasets.

The accuracy of land cover classification from the Random Forest (RF) technique from optical imagery was superior to the results of the maximum likelihood classifier, which is one of the most common classification methods (Rodriguez-Galiano et al. 2012). RF is an ensemble learning technique that builds multiple trees based on random bootstrapped samples of the training data (Breiman 2001). Each tree is built using a different subset from the original training data, containing about two thirds of the cases, and the nodes are split using the best split variable out of a group of randomly selected variables (Liaw and Wiener 2002). This strategy provides robustness to over-fitting and can handle thousands of dependent and independent input variables without variable deletion. The output is determined by a majority vote of the trees. The two user-defined parameters are the number of trees (k) and the number of variables used to split the nodes (m). If the number of trees is increased, the generalization error always converges, and over-training is not a problem. On the other hand, a reduction in the number of predictor variables results in each individual tree of the model being weaker. Therefore, picking a large number of trees is recommended, as well as using the square root of the number of variables used to split the node for the value of m (Breiman 2001). The samples which are not present in the training subset are included as part of another subset called out-of-bag (OOB). These OOB elements, which are not considered for the training of the tree, can be classified by the tree to evaluate performance. The ratio between the misclassifications and the total number of OOB elements contributes an unbiased estimation of the generalization error (Rodriguez-Galiano et al. 2012). RF uses the Gini Index as a measure to identify the best split selection. This index measures the impurity of a given element with respect to the rest of the classes. Data with a higher Gini Index is more important for discrimination. By using a given combination of features, a decision tree can thus grow up to its maximum depth with no pruning. These classifications algorithms were applied using the statistical software R (R Core Team 2013).

The classification maps were evaluated in terms of their overall accuracy (OA), producer's accuracy (PA), and user's accuracy (UA). Furthermore, measures of quantity disagreement (QD) and allocation disagreement (AD) were used for evaluation. The QD is defined as the difference between the reference data and the classified data based upon mismatch of class proportions. AD can be considered as the difference between the classified data and the reference data due to incorrect spatial allocations of pixels in the classification. The total disagreement is the sum of QD and AD (Baker et al, 2013; Pontius and Millones 2011). These measures are much more useful to summarize a cross-tabulation matrix than the kappa index of agreement. In order to compare the accuracy of classification methods, McNemar's test (Hartfield et al., 2013; McNemar 1947) or Z-test (Baker et al., 2012; Congalton and Green 2008; Laurin et al., 2013) were used. McNemar's test takes into account the use of no independent samples by focusing on how each point was either correctly or incorrectly classified in the two classifications being compared. A chi-squared value ≥ 3.84 indicates a significantly different overall accuracy between the two methods at the 95% level of significance. The Z test offers two types of information. First, it determines whether the independently computed kappa is better than one from a random model. Second, it determines whether two independently computed kappas are significantly different (Benjankar et al., 2010). The value of Z score is an approximation of the standard normal deviate of 1.96 for the 95% two-sided confidence level. Since, the purpose is to reveal the best algorithm for crop type classification in this study, the Z-test was performed for a pairwise comparison of the proposed methods.

3. Results and discussion

3.1. Time-Series plot of TerraSAR-X- derived information

Figure 2 shows the temporal patterns of the gamma nought values. A decrease in HH polarization was found from July 31 to August 11 (Figure 2 (a)). However, this was not found for VV polarization in the winter wheat fields (Figure 2 (b)). Although the growth stage was the period of maturity, most winter wheat plants suffered from lodging by a heavy rainfall (Figure 3).It has been shown that the HH polarized wave penetrates a canopy more deeply than the VV polarized wave. Sonobe et al. (2014b) reported a depth of 59.3 cm for VV polarization and of 75.7 cm for HH polarization in winter wheat. A decrease in the thickness of the canopy by lodging was thus connected to an increased influence of the topsoil in HH polarization compared to VV polarization in our results.

Figure 4 shows the temporal patterns of the coherence values. Coherence values in the period from late June to mid-August were low for both HH (Figure 4 (a)) and VV polarization (Figure 4 (b)). Since crop body growth is most pronounced during this period, the satellite return frequency of 11 days was too long to maintain high complex correlation values. In addition, coherence in winter wheat fields and grassland showed low values (~0.4) until harvest season because the crops had been planted in the previous year.

Figure 5 shows the temporal patterns of the polarimetric parameters. Crops were mostly distributed over Z5 and Z6, which supports previous results. In potato fields, direct reflections from the pronounced furrow ridges (30–35 cm in height) resulted in a simple scattering pattern and a noticeable concentration of data in Z8. During early growth periods and post-harvest periods, bare soil fields increased in extent and data was distributed over Z8 in a similar manner.

The period from June 28 to July 9 was marked by only a small amount of precipitation (11 mm on June 4), causing desiccation and leading to a decrease in the height of sugar beet plants in spite of the growth period. As a result, the component of the surface scattering increase around July 9, leading to a decrease of entropy values and an increase in data distribution over Z8.

3.2. Separability assessments

Figure 6 presents the chronological changes for the J-M distance of gamma nought values. The data acquired from June 17 to September 24 was especially useful. Values for the pairs of beans-beet, beans-grassland, beans-wheat, beet-grassland, beet-maize, beet-potato, grassland-maize, grassland-potato, maize-wheat and potato-wheat were over 1.7. This separability was available for both polarizations (Figure 6 (a), (b)). In contrast, values were lower than 1.0 for beans-maize, beans-potato, grassland-wheat and maize-potato. These combinations were more difficult to separate in single polarization data acquired on a specific observation day. A decrease in the J-M distance for many crop combinations was observed due to the rainfall on July 31.

Figure 7 presents the chronological changes in the J-M distance of the coherence values. Values were lower than for gamma nought and at no point larger than 1.0 for beans-beet, beats-grassland, beans-maize, beans-potato, beans-grassland, beet-maize, beet-potato, beet-wheat, grassland-maize, grassland-potato, grassland-wheat, maize-potato, maize-wheat and potato-wheat, for both polarizations (Figure 7 (a) and (b)). In the growth period, coherence values were low for all six crop types due to their high crop height and elongation.

Figure 8 presents the chronological changes for the J-M distance of the polarimetric parameters. The values for entropy (Figure 8 (b)) showed slightly better separability than those for averaged alpha angle (Figure 8 (a)). It is likely that the proportions of the scattering patterns from plant bodies were changed with the growth of the crops, although the types of scattering patterns were relatively constant during the growth period. The low selectivity of the average alpha angle for the last growth period was caused by the approximately equal scattering pattern observed for all crops. The average alpha angle value observed from May 15 to August 31 was particularly effective for classification. Some J-M distances for beans-winter wheat, sugar beet-winter wheat, corn-winter wheat, and potato-winter wheat were larger, yet always below 1.7. A similar tendency was seen for the entropy values and for the separabilities between beans-maize, beans-potato and grassland-winter wheat.

3.3. Parameters of Classifiers

The application of SVM and RF required parameter tunings. For SVM, the optimal values of the two parameters, C and γ, were examined. Figure 9 shows the relationship between these two parameters and the averaged error rate calculated using a 10-fold cross validation. This includes (a) gamma nought, (b) coherence, (c) polarimetric parameters (averaged alpha angle and entropy), (d) the combination of gamma nought and coherence, (e) the combination of gamma nought and polarimetric parameters and (f) the combination of gamma nought, coherence, and polarimetric parameters. In this study, the γ values influenced more than the C values. The optimal parameter pairs were $(2^{-10}, 2^{8})$ for (a), $(2^{-6}, 2^{3})$ for (b), $(2^{-5}, 2^{0})$ for (c), $(2^{-7}, 2^{3})$ for (d), $(2^{-8}, 2^{2})$ for (e) and $(2^{-8}, 2^{1})$ for (f). Since the error rate of (b) was relatively high, the colour scale differs from others. The higher accuracy observed in the central range of C and γ indicates that nearly the same power combination is suitable except (b). Visually, the difference of the distributions is not clear between (e) and (f) and that may imply there is no advantage of adding coherence to gamma nought and polarimetric parameters.

When applying the RF technique, increasing the number of trees causes the generalization error to converge; thus over-training is not a problem (Breiman 1996). Figure 10 indicates that the minimum useful number of trees is approximately 50. In this study, 50 was chosen as the number of trees for all cases. The number of trees should be taken large enough in order to allow for convergence of the OOB error, especially, in case of the separabilities are low for the inputs. Since the number of trees was a fourth part of some studies using multispectral SPOT 5 image (Ok et al., 2012) or EMISAR imagery (Loosvelt et al., 2012), a stable accuracy can be expected from the classification using the multitemporal TerraSAR-X dual-polarimetric data. Figure 11 shows the relative importance of the contribution to the RF classification model for the combination of gamma nought, coherence and polarimetric parameters. According to the Gini index, the features with the greatest contribution to the classification model were the data that were acquired from June to August. In this period, all types of crops were cultivated and the influence of the soil could be ignored for all fields, while the SAR data had a high sensitivity to soil moisture or roughness due to sparse vegetation cover before June (seedlings or transplanting of beans, beet and maize) and after August (the harvest season of winter wheat). Coherence was of low importance, while gamma nought and polarimetric parameters were particularly effective for classification.

3.4. Accuracy Validation

The corresponding confusion matrices of classifications using TerraSAR-X data are given in Table 4. For all algorithms, classification results of (e) were superior to the other combinations. When coherence was added to gamma nought, overall accuracy increased from 89.7% to 90.5%. When coherence was added to gamma nought and polarimetric values, overall accuracy increased from 93.8 to 94.4. Furthermore, the OOB error decreased (Figure 9). However, the advantages of using coherence were not confirmed at the 95% level of significance.

In all of the information derived from the TerraSAR-X data and algorithms used in this study, the discrimination precision for winter wheat and sugar beet were higher than for the other four kinds of crops. Even though J-M distances were lower than 1.0 on all TerraSAR-X acquisition days, good results were achieved (e.g., separability between winter wheat and grass) due to the characteristics of the machine learning algorithm. When the coherence data were used, overall accuracy was 75.7% for SVM, 77.0% for RF and 68.5% for CART, respectively, which is lower than the accuracy for the other TerraSAR-X-derived information. On the other hand, an overall accuracy of more than 90% was confirmed for applying SVM to backscattering coefficient, and SVM or RF to polarimetric parameters. This supports the separability results discussed in the previous section. In addition, PA and UA for maize were lower than for other crops. This result agrees with an earlier study which applied RF to backscattering coefficient (Sonobe et al. 2014a). Using polarimetric parameters did however lead to improvements in precision. For all algorithms, classification results using gamma nought and polarimetric parameters were superior to those using other parameters. No advantages of using coherence were confirmed.

3.5. Statistical comparison

A Z-test was used to compare classification accuracy among the different types of TerraSAR-X-derived information. Table 5 (a) shows the results for CART, Table 5 (b) for SVM and Table 5 (c) for RF. To be significantly different at the 95% confidence level, the absolute value of the Z score should be >1.96, and this happened for 11 inputs out of 15 using CART, 12 inputs out of 15 using SVM and 13 inputs out of 15 using RF. Except RF, the differences between the classification results of gamma nought, and that of polarimetric parameters were not meaningful. And There are no meaningful differences between the classification results of gamma nought and that of gamma nought and coherence except CART.

Furthermore, no meaningful differences were observed between the classification results using all TerraSAR-X-derived information and those using gamma nought and polarimetric parameters only for all algorithms. The applicability of coherence in crop classification therefore remains unclear, while the combination of gamma nought and polarimetric parameters appears to be effective for this purpose.

A Z-test was also used to compare the accuracy of the classification results for each classification technique when gamma nought and polarimetric parameters were used. Z-scores are shown in Table 6. Results indicate that the SVM classifier using gamma nought and polarimetric parameters provided the highest quality crop classification map in this study area. Figure 12 shows the crop classification map, with misclassified fields outlined in red. The most of the misclassifications happened in the small fields. Since grasslands have large area and more grasslands were located in the northern part, more misclassifications were observed in the southern part than in the northern part. There were 202 misclassified fields, consisting of 55 bean fields (6.7% of total beans fields in the test data), 17 sugar beet fields (3.4%), 20 grasslands (4.0%), 39 maize fields (8.2%), 32 potato fields (5.7%) and 39 winter wheat fields (3.2%). Figure 13 shows the relationship between field area and misclassified field. 43.6–62.5% of the misclassified fields were less than 100 a in area and 79.5–96.3% were less than 200 a (with the exception of grassland). When some feature such as a road or windbreak forest is present in the TerraSAR-X data, the ratio of its extent to that of the field is relatively higher for the smaller fields, which leads to misclassifications. However, misclassifications were found in fields larger than 222 a (the mean of included field areas), and were outstanding for grassland in particular. After the harvest of grass, roll veils are often left in the fields and may cause strong directional reflection, which leads to high gamma nought values. Furthermore, harvesting periods varied among grassland fields, causing unevenness in growth and influencing scattering patterns.

4. Conclusions

Analytical techniques using SAR data include interferometric SAR and polarimetric SAR in addition to the use of backscattering coefficients such as gamma nought. These techniques are capable of acquiring information about the shape and changes of a target area by employing multi-temporal SAR data. This study demonstrated the great potential of TerraSAR-X HH and VV polarization data operated in StripMap mode for agricultural applications. Sixteen acquisitions and their corresponding gamma nought, averaged alpha angle and scattering entropy values were analyzed together with *in situ* measurements. The high sensitivity of gamma nought to crop height was demonstrated statistically for beans, beet and maize. In addition, comparisons were conducted among the CART, SVM and RF algorithms. The SVM classifier using gamma nought and polarimetric parameters was found to be able to generate the best crop classification map of the monitored study area with an overall accuracy of 95.0%.

Acknowledgments

The authors are thankful to Tokachi Nosai for providing the field data. This work was supported by JSPS KAKENHI Grant Number 26・5253.

References

Ager, T.P., & Bresnahan, P.C. (2009). Geometric precision in space radar imaging: results from TerraSAR-X. In, *ASPRS 2009 annual conference* (pp. 9-13). Baltimore, Maryland, USA

Baker, B. A., Warner, T. A., Conley, J.F., & McNeil, B. E. (2013). Does spatial resolution matter? A multi-scale comparison of object-based and pixel based methods for detecting change associated with gas well drilling operations. *International Journal of Remote Sensing*, *34*, 1633-1651

Bargiel, D., & Herrmann, S. (2011). Multi-temporal land-cover classification of agricultural areas in two European regions with high resolution Spotlight TerraSAR-X data. *Remote Sensing, 3*, 859-877

Benjankar, R., Glenn, N.F., Egger, G., Jorde, K., & Goodwin, P. (2010). Comparison of Field-Observed and Simulated Map Output from a Dynamic Floodplain Vegetation Model Using Remote Sensing and GIS Techniques. GIScience & Remote Sensing, 47, 480-497

Blaes, X., & Defourny, P. (2003). Retrieving crop parameters based on tandem ERS 1/2 interferometric coherence images. *Remote Sensing of Environment, 88*, 374-385

Bovolo, F., Bruzzone, L., & Carlin, L. (2010). A novel technique for subpixel image classification based on support vector machine. *IEEE Transactions on Image Processing, 19*, 2983-2999

Breiman, L. (1996). Bagging predictors. *Machine Learning, 24*, 123-140

Breiman, L. (2001). Random forests. *Machine Learning, 45*, 5-32

Chang, C., Chien, L., & Lee, Y. (2011). A novel framework for multi-class classification via ternary smooth support vector machine. *Pattern Recognition, 44*, 1235-1244

Choudhury, I., & Chakraborty, M. (2006). SAR signature investigation of rice crop using RADARSAT data. *International Journal of Remote Sensing, 27*, 519-534

Congalton, R.G., & Green, K. (2008). *Assessing the Accuracy of Remotely Sensed Data: Principles and Practices*. Boca Raton, Florida, United States: CRC Press

Duro, D., Franklin, S., & Dube, M. (2012). Multi-scale object-based image analysis and feature selection of multi-sensor earth observation imagery using random forests. *International Journal of Remote Sensing, 33*, 4502-4526

Fontanelli, G., Paloscia, S., Zribi, M., & Chahbi, A. (2013). Sensitivity analysis of X-band SAR to wheat and barley leaf area index in the Merguellil Basin. *Remote Sensing Letters, 4*, 1107-1116

Foody, G., & Mathur, A. (2004). A relative evaluation of multiclass image classification by support vector machines. *IEEE Transactions on Geoscience and Remote Sensing, 42*, 1335-1343

Gebhardt, S., Huth, J., Nguyen, L., Roth, A., & Kuenzer, C. (2012). A comparison of TerraSAR-X Quadpol backscattering with RapidEye multispectral vegetation indices over rice fields in the Mekong Delta, Vietnam. *International Journal of Remote Sensing, 33*, 7644-7661

Gens, R., Atwood, D., & Pottier, E. (2013). Geocoding of polarimetric processing results: Alternative processing strategies. *Remote Sensing Letters, 4*, 39-45

Gens, R., & Logan, T. (2003). *Alaska Satellite Facility Software Tools: Manual*. Geophysical Institute, University of Alaska Fairbanks

Gislason, P., Benediktsson, J., & Sveinsson, J. (2006). Random Forests for land cover classification. *Pattern Recognition Letters, 27*, 294-300

Hartfield, K., Marsh, S., Kirk, C., & Carriere, Y. (2013). Contemporary and historical classification of crop types in Arizona. *International Journal of Remote Sensing, 34*, 6024-6036

Kavzoglu, T., & Colkesen, I. (2013). An assessment of the effectiveness of a rotation forest ensemble for land-use and land-cover mapping. *International Journal of Remote Sensing, 34*, 4224-4241

Koppe, W., Gnyp, M., Hutt, C., Yao, Y., Miao, Y., Chen, X., & Bareth, G. (2013). Rice monitoring with multi-temporal and dual-polarimetric TerraSAR-X data. *International Journal of Applied Earth Observation and Geoinformation, 21*, 568-576

Kuenzer, C., & Knauer, K. (2013). Remote sensing of rice crop areas. *International Journal of Remote Sensing, 34*, 2101-2139

Laurin, G.V., Frate, F.D., Pasolli, L., Notarnicola, C., Guerriero, L., & Valentini, V. (2013).

Discrimination of vegetation types in alpine sites with ALOS PALSAR-, RADARSAT-2-, and lidar-derived information, *International Journal of Remote Sensing, 34*, 6898-6913

Liaw, A., & Wiener, M. (2002). Classification and regression by random Forest. *R News, 2*, 18-22

Liesenberg, V., & Gloaguen, R. (2013). Evaluating SAR polarization modes at L-band for forest classification purposes in Eastern Amazon, Brazil. *International Journal of Applied Earth Observation and Geoinformation, 21*, 122-135

Liu, B., Hu, H., Wang, H., Wang, K., Liu, X., & Yu, W. (2013). Superpixel-based classification with an adaptive number of classes for polarimetric SAR images. *IEEE Transactions on Geoscience and Remote Sensing, 51*, 907-924

Lizarazo, I. (2008). SVM-based segmentation and classification of remotely sensed data. *International Journal of Remote Sensing, 29*, 7277-7283

Loosvelt, L., Peters, J., Skriver, H., De Baets, B., & Verhoest, N. (2012). Impact of Reducing Polarimetric SAR Input on the Uncertainty of Crop Classifications Based on the Random Forests Algorithm. *IEEE Transactions on Geoscience and Remote Sensing, 50*, 4185-4200

Lopez-Sanchez, J., Cloude, S., & Ballester-Berman, J. (2012). Rice Pphenology monitoring by means of SAR polarimetry at X-Band. *IEEE Transactions on Geoscience and Remote Sensing, 50*, 2695-2709

Macelloni, G., Paloscia, S., Pampaloni, P., Marliani, F. , & Gai, M. (2001). The relationship between the backscattering coefficient and the biomass of narrow and broad leaf crops. *IEEE Transactions on Geoscience and Remote Sensing*, 39, 873-884

McNemar, Q. (1947). Note on the Sampling Error of the Difference between Correlated Proportions or Percentages. *Psychometrika 12*, 153-157

Mishra, N.B., & Crews, K.A. (2014). Mapping vegetation morphology types in a dry savanna ecosystem: integrating hierarchical object-based image analysis with Random Forest. *International Journal of Remote Sensing, 35*, 1175-1198

Ok, A.O., Akar, O., & Gungor, O. (2012). Evaluation of random forest method for agricultural crop classification. *European Journal of Remote Sensing*, 45, 421-432

Pal, M. (2005). Random forest classifier for remote sensing classification. *International Journal of Remote Sensing, 26*, 217-222

Pal, M. (2008). Ensemble of support vector machines for land cover classification. *International Journal of Remote Sensing, 29*, 3043-3049

Pontius, R., & Millones, M. (2011). Death to Kappa: birth of quantity disagreement and allocation disagreement for accuracy assessment. *International Journal of Remote Sensing, 32*, 4407-4429

Pottier, E., Ferro-Famil, L., Allain, S., Cloude, S.R., Hajnsek, I., Papathanassiou, K., Moreira, A., Williams, M., Minchella, A., Lavalle, M., & Desnos, Y.L. (2009). *Overview of the PolSARpro v4.0: the open source toolbox for polarimetric and interferometric polarimetric SAR data processing*. In, *IGARSS 2009* (pp. 936-939). Cape Town, South Africa

Puertas, O., Brenning, A., & Meza, F. (2013). Balancing misclassification errors of land cover classification maps using support vector machines and Landsat imagery in the Maipo river basin (Central Chile, 1975-2010). *Remote Sensing of Environment, 137*, 112-123

Richards, J.A. (1999). *Remote Sensing Digital Image Analysis*. Berlin: Springer-Verlag

Rodriguez-Galiano, V., Chica-Olmo, M., Abarca-Hernandez, F., Atkinson, P., & Jeganathan, C. (2012). Random Forest classification of Mediterranean land cover using multi-seasonal imagery and multi-seasonal texture. *Remote Sensing of Environment, 121*, 93-107

Roth, A., Huber, M., & Kosmann, D. (2004). Geocording of TerraSAR-X data. In, *20th ISPRS Congress* (pp. 840-844). Istanbul

Sarker, L., & Nichol, J. (2011). Improved forest biomass estimates using ALOS AVNIR-2 texture indices. *Remote Sensing of Environment, 115*, 968-977

Sonobe, R., Tani, H., Wang, X., Kobayashi, N., & Shimamura, H. (2014a). Random forest classification of crop type using multi-temporal TerraSAR-X dual-polarimetric data. *Remote Sensing Letters, 5*, 157-164

Sonobe, R., Tani, H., Wang, X., Kobayashi, N., & Shimamura, H. (2014b). Winter wheat growth monitoring using multi-temporal TerraSAR-X dual-polarimetric data. *Japan Agricultural Research Quarterly, 48,* 471-476

Uhlmann, S., & Kiranyaz, S. (2014). Integrating Color Features in Polarimetric SAR Image Classification. *IEEE Transactions on Geoscience and Remote Sensing, 52*, 2197-2216

Table

Table 1. Cultivation calendar for the crops in this study area.

Table 2 Crop type and number of fields.

Table 3 Characteristics of the satellite data.

Table 4 Accuracy results.

Table 5 Z-test results for TerraSAR-X-derived information.

Table 6 Z-test results for CART, SVM and RF.

Figure

Figure 1 Overview of the data processing.

Figure 2 Temporal variation of gamma nought values.

Figure 3 Damaged winter wheat field. Photographed on August 1, 2013

Figure 4 Temporal variation of gamma coherence.

Figure 5 Temporal variation of polarimetric parameters.

Figure 6 Jeffries-Matusita distances for gamma nought.

Figure 7 Jeffries-Matusita distances for coherence.

Figure 8 Jeffries-Matusita distances for polarimetric parameters

Figure 9 Results of 10-fold cross-validation for SVM classification of the training data.

Figure 10 Relationships between number of trees and error rate for OOB samples.

Figure 11 Importance of data acquisition date based on Gini measures.

Figure 12 Crop classification map.

Figure 13 Relationship between field area and misclassified fields.

Table 1. Cultivation calendar for the crops in this study area.

		May		June			July			August			September			October	
		late	early	mid	late	early	mid	late	early	mid	late	early	mid	late	early	mid	late
Beans	Azuki	sowing		sprouting												harvesting	
	Soy	sowing		sprouting													harvesting
Beet																harvesting	
Grassland			appearance of ears of grain		first harvesting						second harvesting						
Maize		sowing							appearance of tassel							harvesting	
Potato		planting		sprouting										harvesting			
Wheat		appearance of ears of grain								harvesting							

Table 2 Crop type and number of fields.

Crop type	No. of fields	
	Training data	Test data
Beans	205	818
Beet	122	494
Grassland	126	503
Maize	119	473
Potato	141	563
Wheat	304	1221

Table 3 Characteristics of the satellite data.

Satellite	Acquisition	Precipitation (mm)
TerraSAR-X	15 May, 2013 08:21'26.021410" (UTC)	0.0
TerraSAR-X	26 May, 2013 08:21'27.113650" (UTC)	0.0
TerraSAR-X	06 June, 2013 08:21'26.972120" (UTC)	0.0
TerraSAR-X	17 June, 2013 08:21'28.577500" (UTC)	3.5
TerraSAR-X	28 June, 2013 08:21'29.086800" (UTC)	0.0
TerraSAR-X	09 July, 2013 08:21'29.596490" (UTC)	0.0
TanDEM-X	20 July, 2013 08:21'30.468880" (UTC)	0.0
TerraSAR-X	31 July, 2013 08:21'31.124660" (UTC)	9.0
TanDEM-X	11 August, 2013 08:21'32.229560"(UTC)	0.0
TanDEM-X	22 August, 2013 08:21'32.437250"(UTC)	0.0
TanDEM-X	02 September, 2013 08:21'32.815840"(UTC)	0.5
TanDEM-X	13 September, 2013 08:21'33.421140"(UTC)	0.0
TanDEM-X	24 September, 2013 08:21'33.753040"(UTC)	0.0
TanDEM-X	05 October, 2013 08:21'33.544700"(UTC)	0.0
TanDEM-X	16 October, 2013 08:21'33.901930"(UTC)	55.0
TanDEM-X	27 October, 2013 08:21'33.731850"(UTC)	0.0

Table 4 Accuracy results.

		TerraSAR-X-derived information					
		(a)	(b)	(c)	(d)	(e)	(f)
CART	Producer's accuracy						
	Beans	0.811	0.660	0.774	0.812	0.779	0.779
	Beet	0.877	0.583	0.739	0.891	0.866	0.866
	Grasslands	0.783	0.640	0.819	0.783	0.839	0.783
	Maize	0.385	0.641	0.662	0.622	0.721	0.721
	Potato	0.785	0.474	0.796	0.760	0.824	0.824
	Wheat	0.947	0.875	0.916	0.947	0.927	0.943
	User's accuracy						
	Beans	0.674	0.684	0.835	0.733	0.934	0.934
	Beet	0.846	0.539	0.713	0.840	0.738	0.738
	Grasslands	0.881	0.638	0.715	0.881	0.823	0.876
	Maize	0.611	0.649	0.751	0.724	0.683	0.683
	Potato	0.781	0.599	0.736	0.818	0.776	0.776
	Wheat	0.913	0.803	0.932	0.913	0.943	0.912
	Overall accuracy	0.803	0.685	0.808	0.829	0.841	0.839
	Kappa	0.754	0.608	0.762	0.787	0.804	0.801
	Allocation disagreement	14.023	27.824	15.864	13.089	12.058	11.469
	Quantity disagreement	5.673	3.708	3.364	4.003	3.856	4.641
SVM	Producer's accuracy						
	Beans	0.885	0.707	0.916	0.883	0.933	0.930
	Beet	0.955	0.684	0.949	0.964	0.966	0.970
	Grasslands	0.954	0.875	0.924	0.952	0.960	0.962
	Maize	0.850	0.628	0.873	0.801	0.918	0.896
	Potato	0.897	0.584	0.929	0.883	0.943	0.945
	Wheat	0.965	0.903	0.963	0.964	0.968	0.970
	User's accuracy						
	Beans	0.894	0.686	0.949	0.876	0.951	0.952
	Beet	0.940	0.788	0.929	0.939	0.968	0.964
	Grasslands	0.894	0.653	0.891	0.907	0.918	0.905
	Maize	0.846	0.686	0.892	0.810	0.891	0.922
	Potato	0.923	0.751	0.899	0.907	0.943	0.925
	Wheat	0.981	0.877	0.971	0.983	0.984	0.982
	Overall accuracy	0.924	0.757	0.932	0.916	0.950	0.949
	Kappa	0.906	0.699	0.916	0.896	0.939	0.937
	Allocation disagreement	6.557	18.615	5.599	7.318	4.052	3.954
	Quantity disagreement	1.081	5.648	1.203	1.081	0.909	1.154

RF	Producer’s accuracy						
	Beans	0.880	0.713	0.910	0.892	0.936	0.932
	Beet	0.939	0.700	0.911	0.943	0.945	0.955
	Grasslands	0.920	0.795	0.909	0.920	0.938	0.940
	Maize	0.710	0.634	0.871	0.738	0.869	0.892
	Potato	0.876	0.680	0.913	0.888	0.927	0.934
	Wheat	0.962	0.921	0.972	0.964	0.969	0.975
	User’s accuracy						
	Beans	0.824	0.725	0.916	0.828	0.932	0.944
	Beet	0.939	0.826	0.922	0.961	0.967	0.967
	Grasslands	0.897	0.760	0.903	0.911	0.909	0.920
	Maize	0.787	0.713	0.888	0.837	0.873	0.881
	Potato	0.901	0.654	0.915	0.891	0.934	0.933
	Wheat	0.968	0.854	0.957	0.966	0.971	0.975
	Overall accuracy	0.897	0.770	0.924	0.905	0.938	0.944
	Kappa	0.872	0.714	0.906	0.882	0.924	0.931
	Allocation disagreement	8.644	19.524	7.024	7.809	5.673	5.133
	Quantity disagreement	1.694	3.463	0.540	1.694	0.491	0.442

Note: (a) gamma nought, (b) coherence, (c) polarimetric parameters (averaged alpha angle and entropy), (d) the combination of gamma nought and coherence, (e) the combination of gamma nought and polarimetric parameters and (f) the combination of gamma nought, coherence, and polarimetric parameters.

Table 5 Z-test results for TerraSAR-X-derived information.

CART

	(a)	(b)	(c)	(d)	(e)	(f)
gamma nought		12.98	0.76	3.19	4.86	4.54
coherence			13.76	16.21	17.95	17.62
polarimetric parameters				2.44	4.10	3.78
gamma nought + coherence					1.65	1.34
gamma nought + polarimetric parameters						0.32

SVM

	(a)	(b)	(c)	(d)	(e)	(f)
gamma nought		21.83	1.47	1.28	5.03	4.72
coherence			23.25	20.57	26.61	26.33
polarimetric parameters				2.75	3.57	3.26
gamma nought + coherence					6.30	5.99
gamma nought + polarimetric parameters						0.31

RF

	(a)	(b)	(c)	(d)	(e)	(f)
gamma nought		16.12	4.45	1.27	6.97	8.09
coherence			20.51	17.38	22.95	24.03
polarimetric parameters				3.18	2.54	3.68
gamma nought + coherence					5.71	6.83
gamma nought + polarimetric parameters						1.14

Note: (a) gamma nought, (b) coherence, (c) polarimetric parameters (averaged alpha angle and entropy), (d) the combination of gamma nought and coherence, (e) the combination of gamma nought and polarimetric parameters and (f) the combination of gamma nought, coherence, and polarimetric parameters.

Table 6 Z-test results for CART, SVM and RF.

	SVM	RF	CART
SVM		2.40	16.76
RF			14.46
CART			

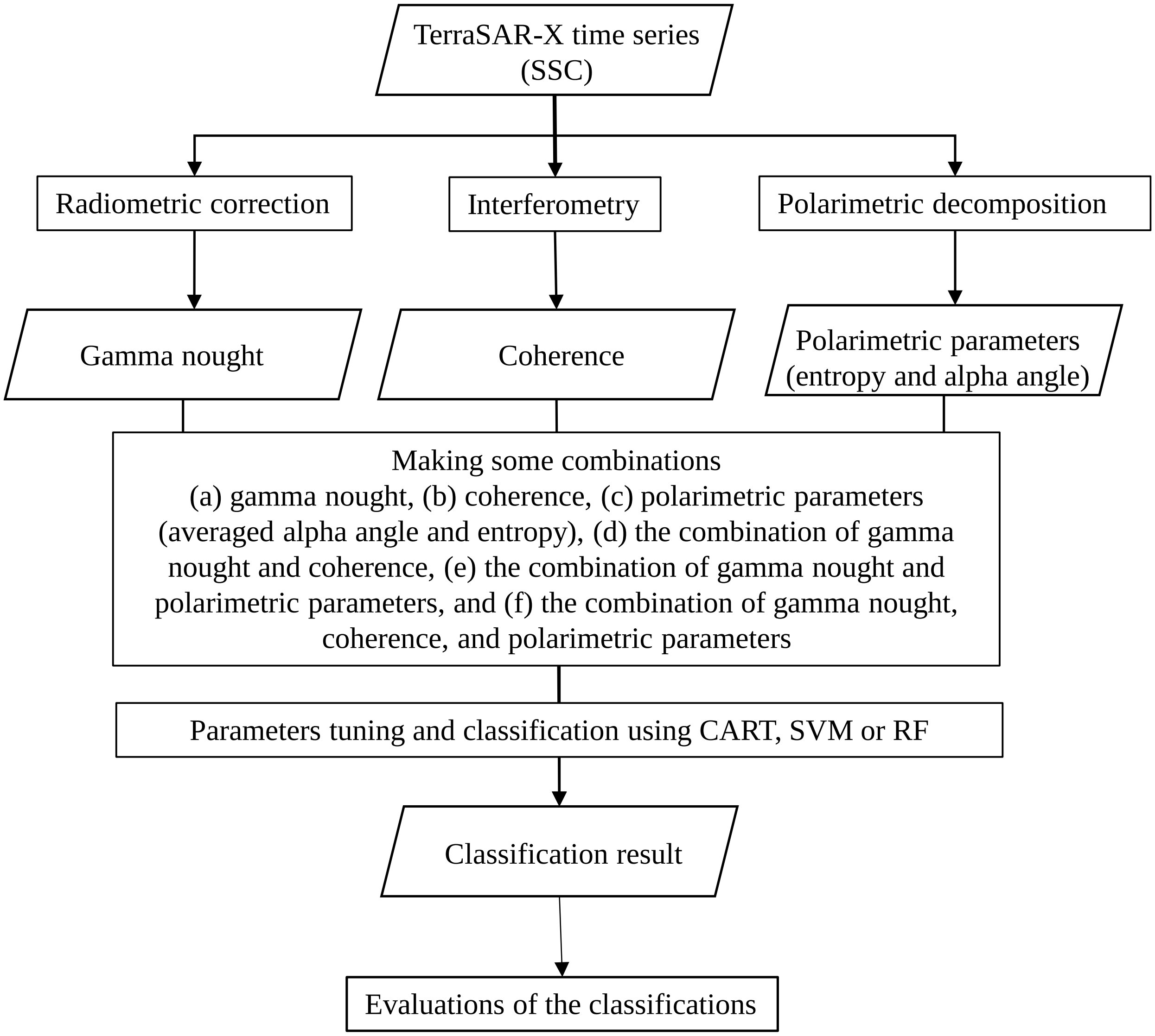

Figure 1. Overview of the data processing.

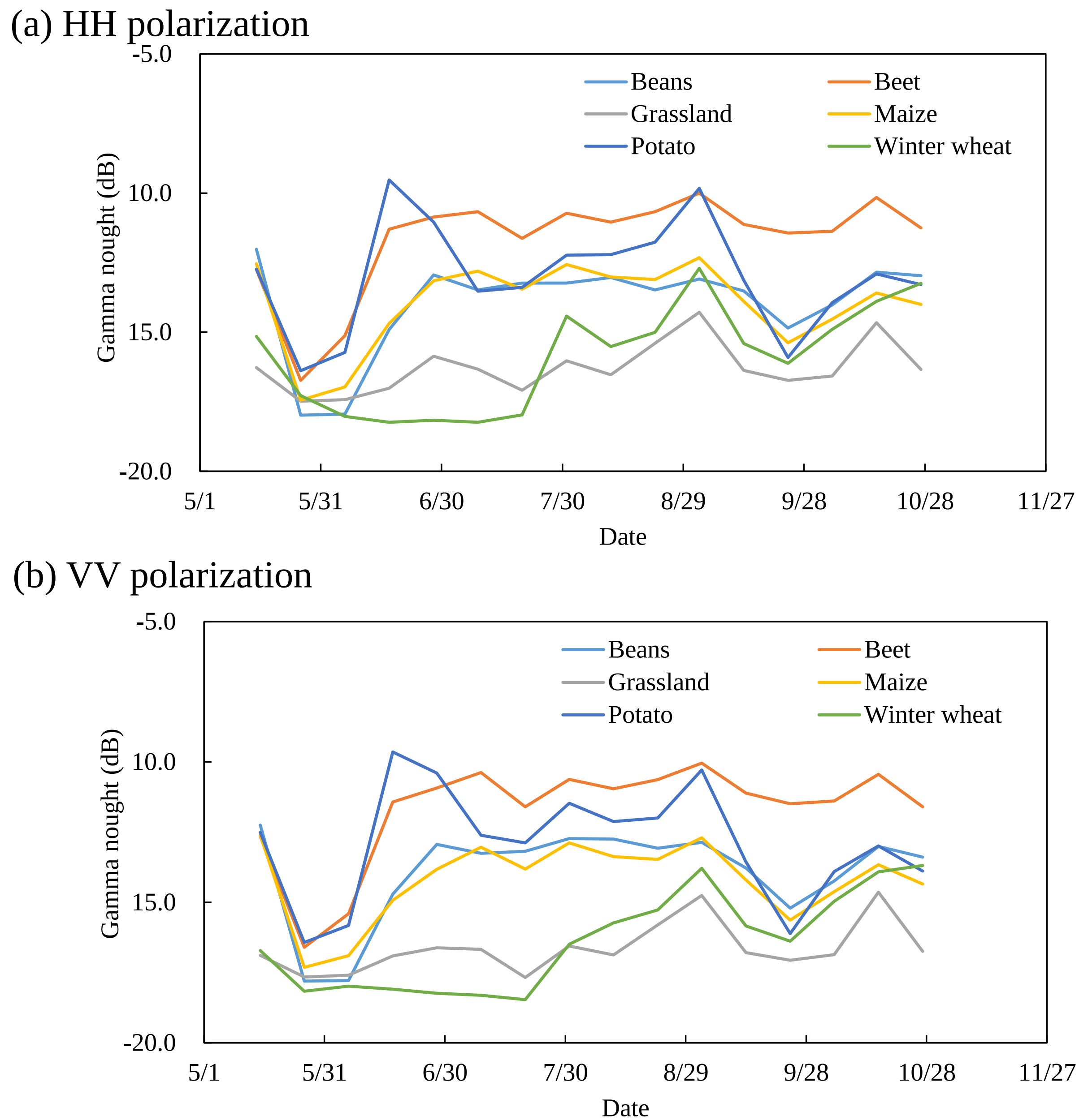

Figure 2 Temporal variation of gamma nought values.

Figure 3 Damaged winter wheat field. Photographed on August 1, 2013

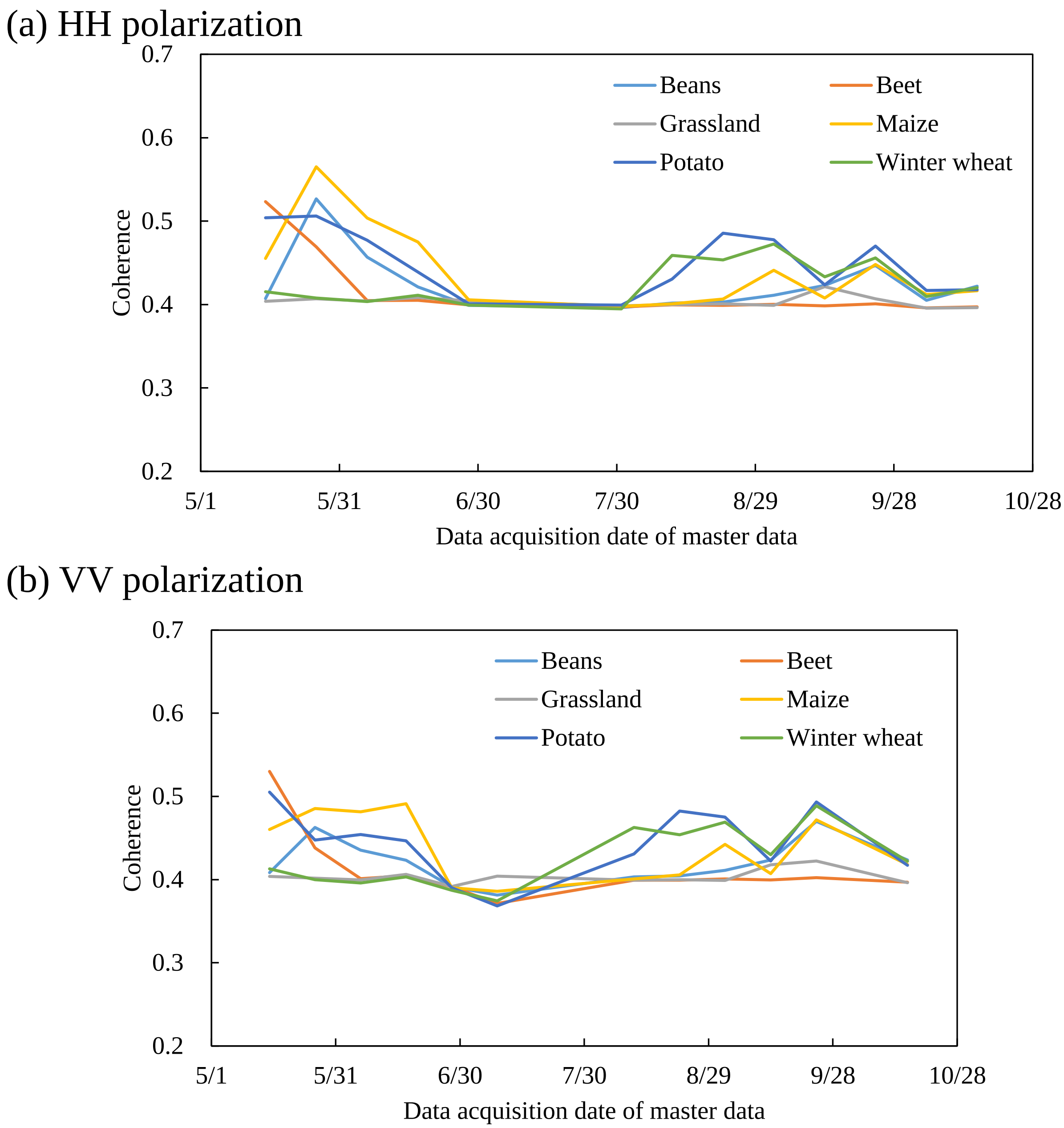

Figure 4 Temporal variation of coherence.

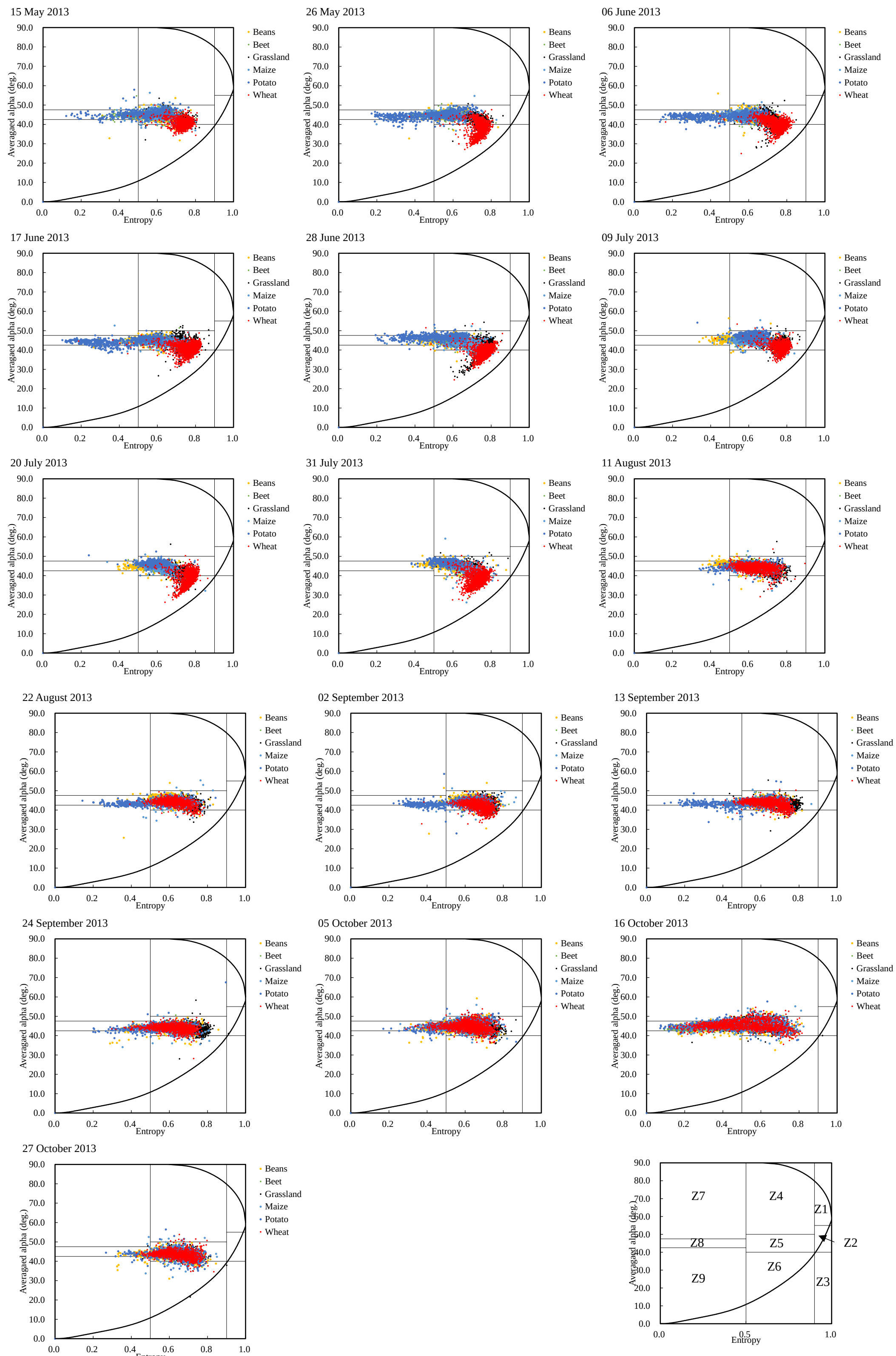

Figure 5 Temporal variation of polarimetric parameters.

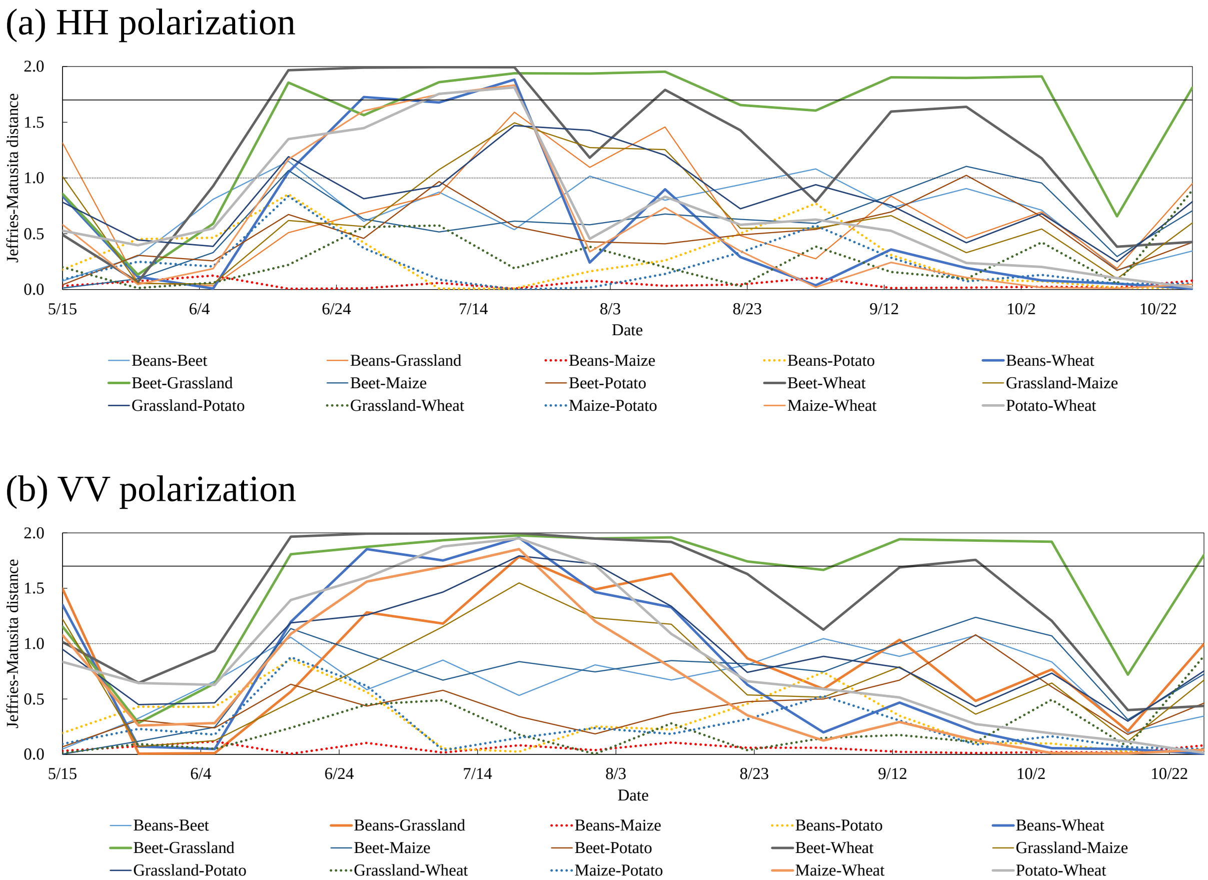

Figure 6 Jeffries-Matusita distances for gamma nought. The thick lines represent the Jeffries-Matusita distances values are greater than 1.7 at least one day, the dotted lines represent below 1.0 in the every observation days.

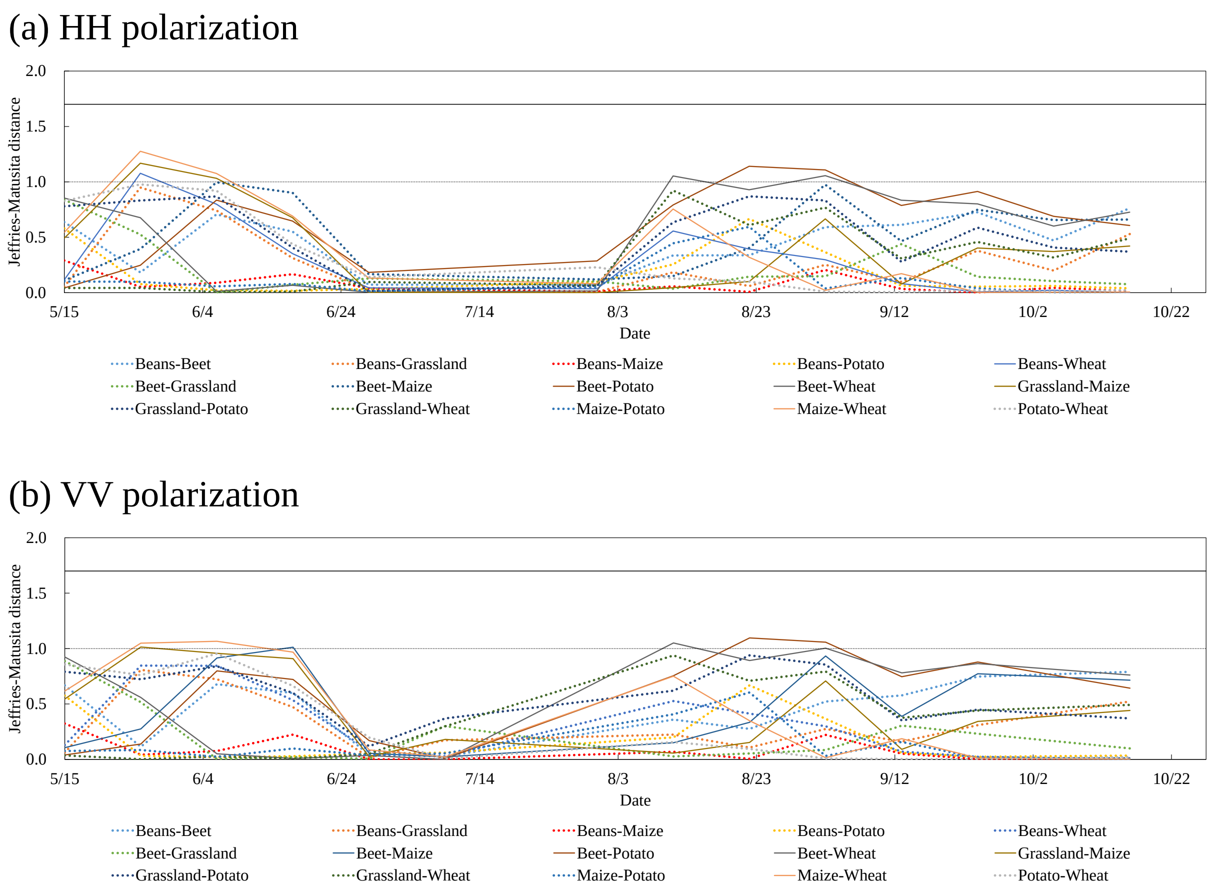

Figure 7 Jeffries-Matusita distances for coherence. The x-axis represents the data acquisitiondate of the master data for coherence. The thick lines represent the Jeffries-Matusita distances values are greater than 1.7 at least one day, the dotted lines represent below 1.0 in the every observation days.

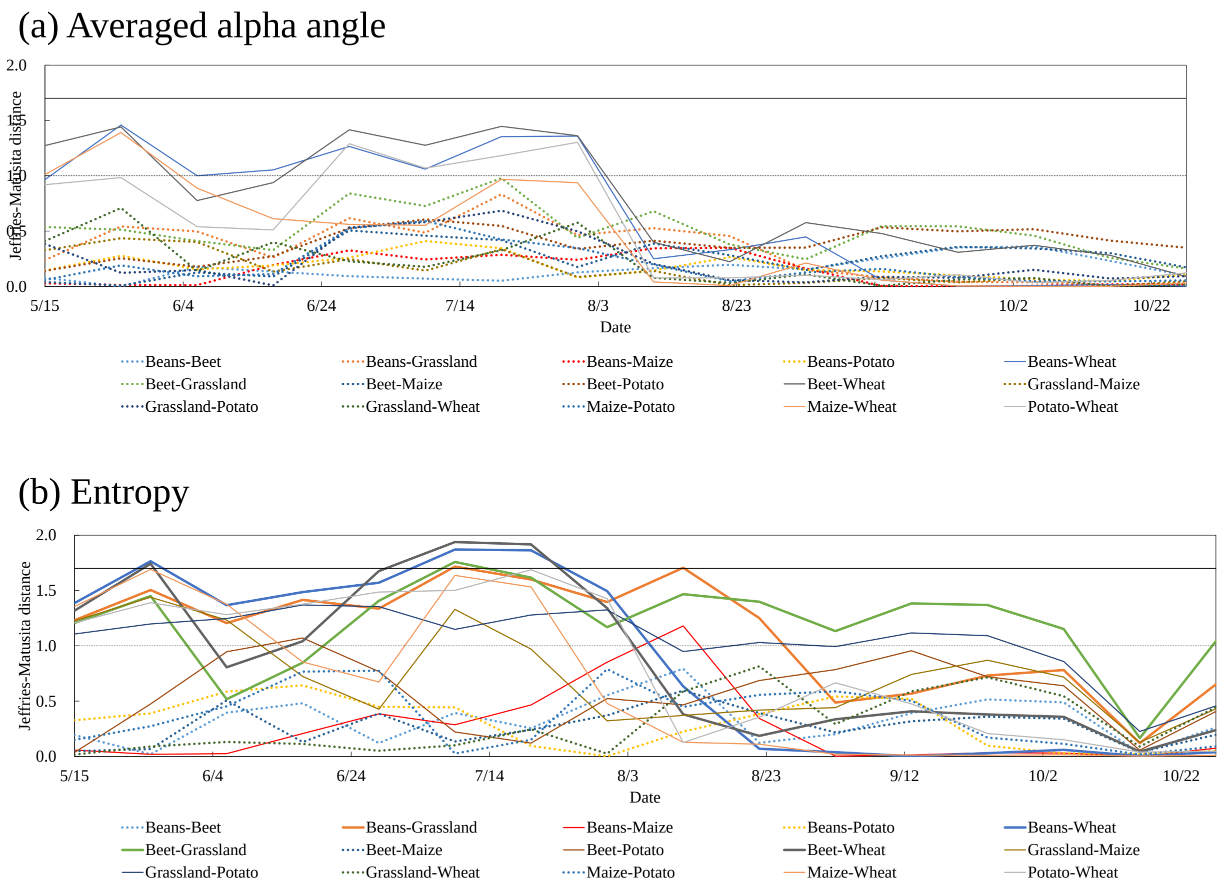

Figure 8 Jeffries-Matusita distances for polarimetric parameters. The thick lines represent the Jeffries-Matusita distances values are greater than 1.7 at least one day, the dotted lines represent below 1.0 in the every observation days.

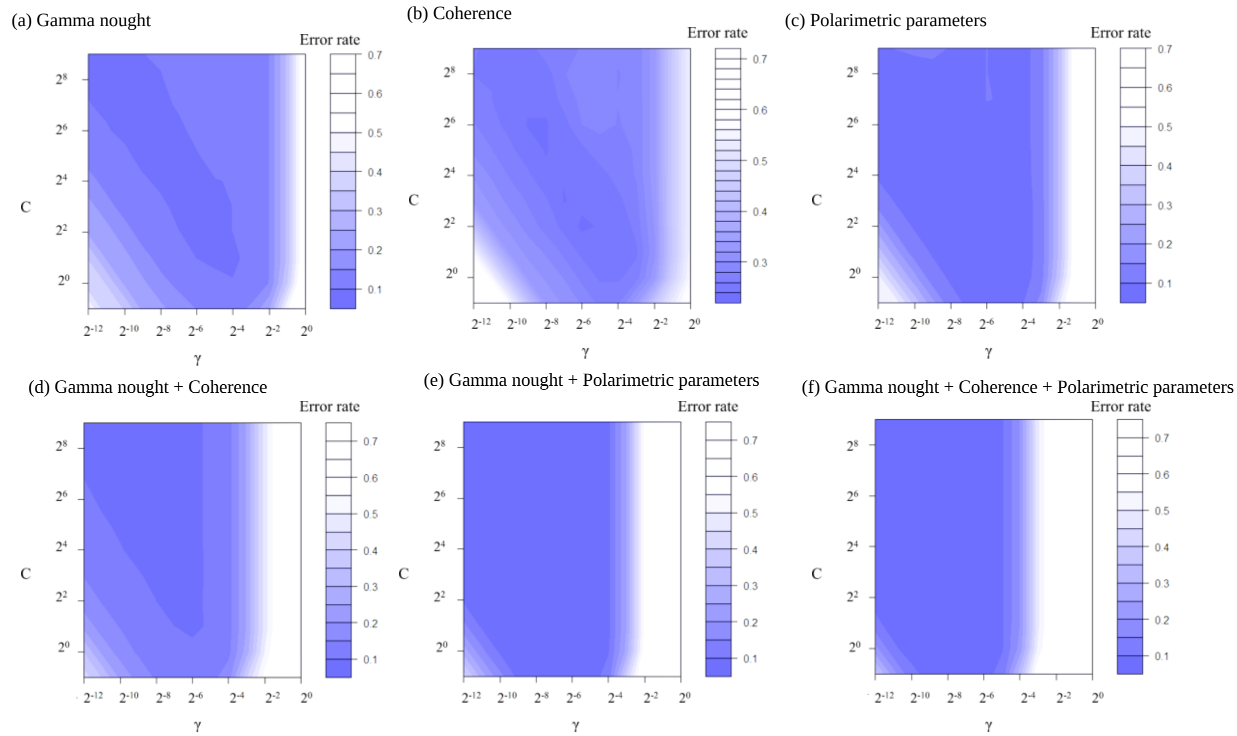

Figure 9 Results of 10-fold cross-validation for SVM classification of the training data.

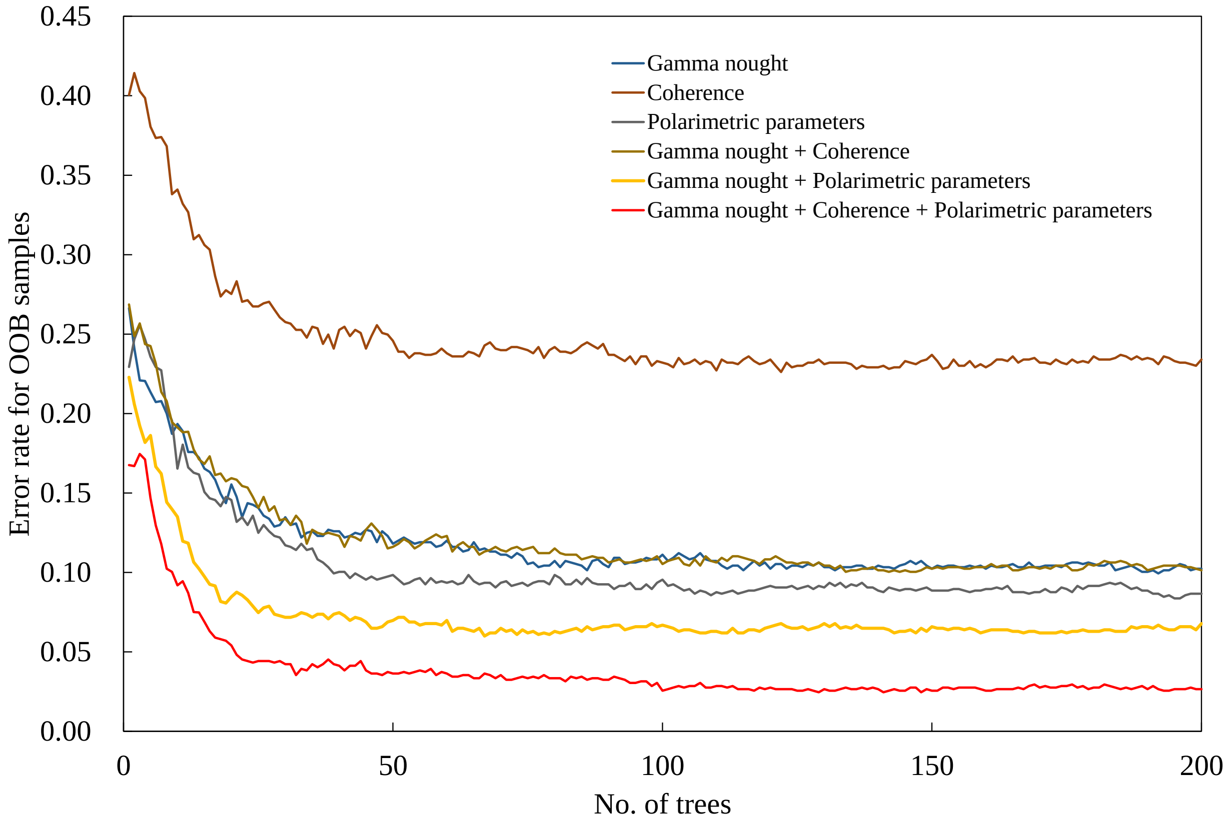

Figure 10 Relationships between number of trees and error rate for OOB samples.

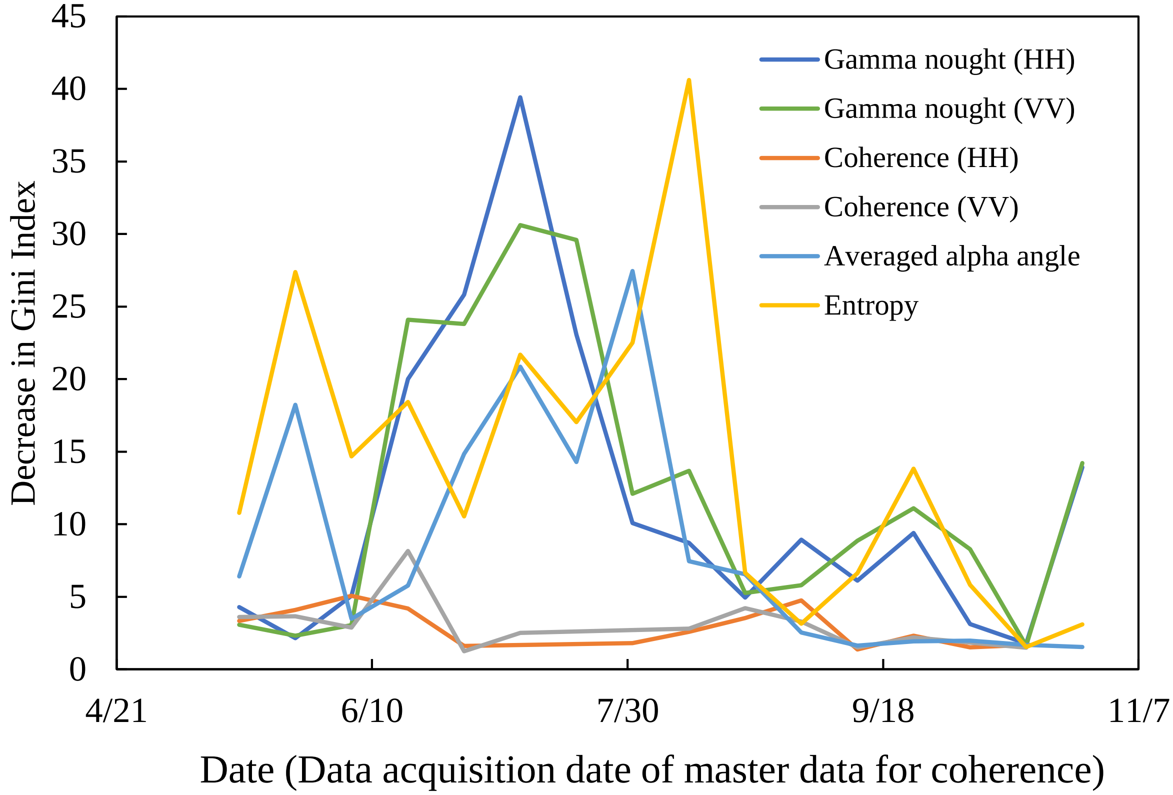

Figure 11 Importance of data acquisition date based on Gini measures.

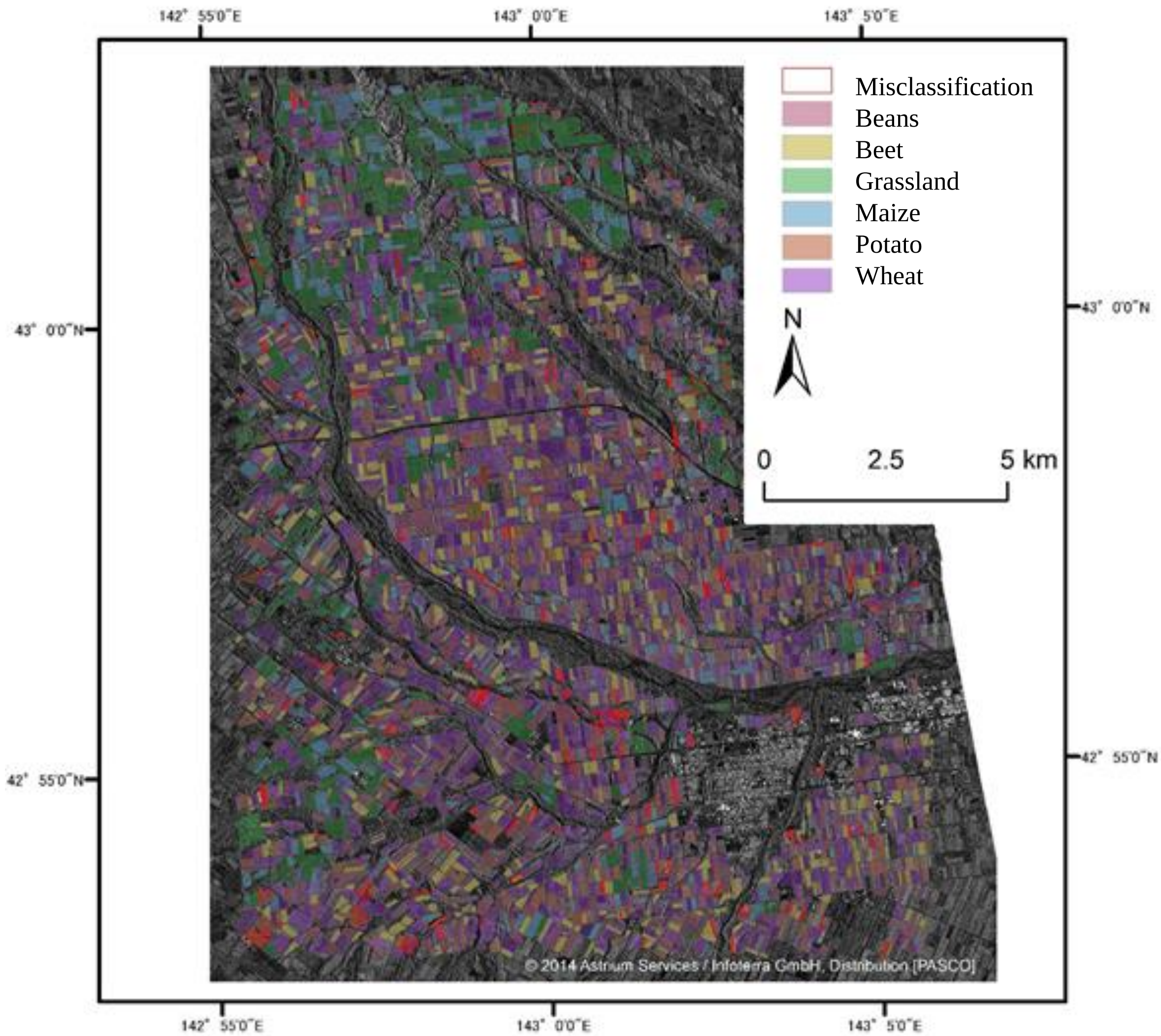

Figure 12 Crop classification map.

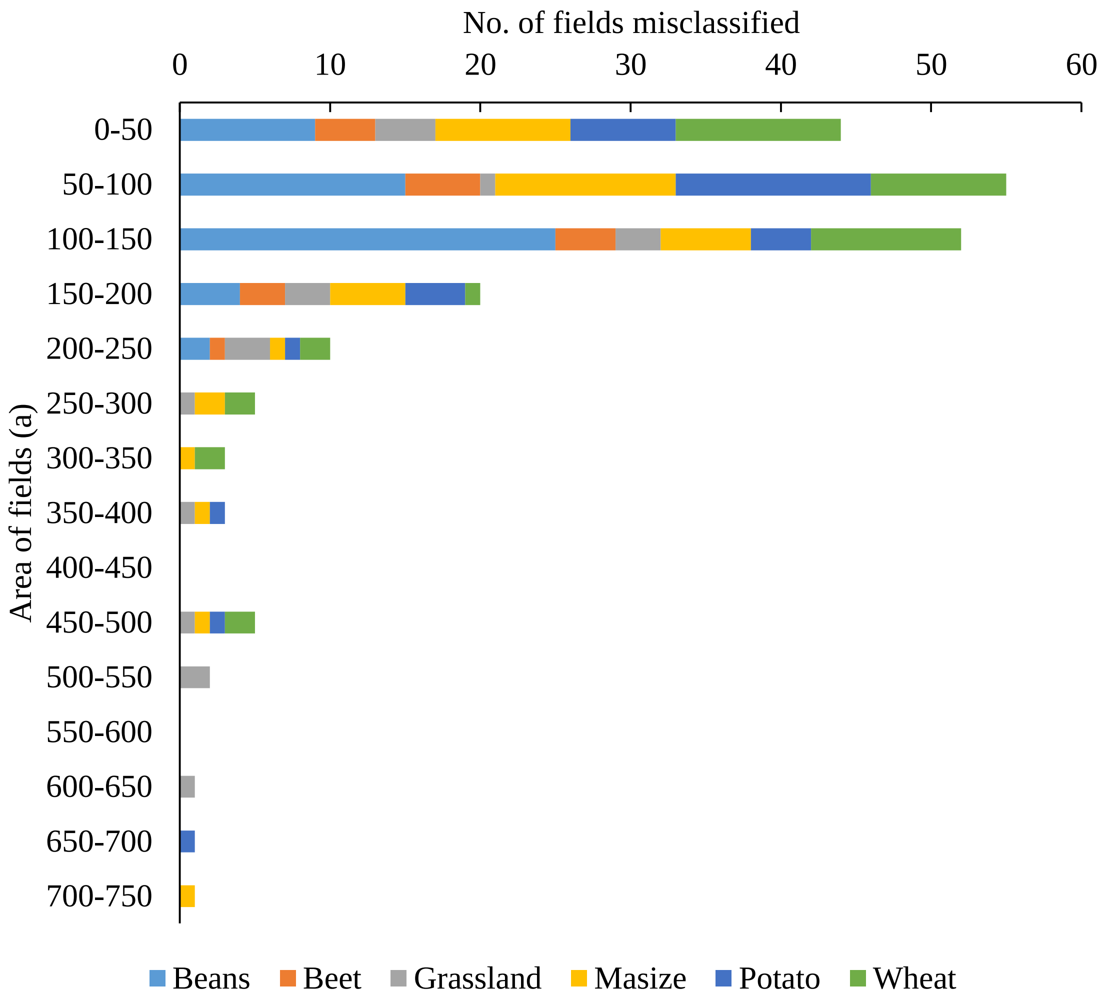

Figure 13 Relationship between field area and misclassified fields.